Analytic Approximations of the Steady State Particle Distribution Function in Rotating Magnetic Mirrors

Greta Li

Program in Plasma Science and Technology (PPST) Summer 2023

1 Introduction

Magnetic mirrors have recently experienced renewed interest as a potential alternative fusion concept. One way of addressing particle loss via diffusion into the mirror loss cone is through rotating the plasma, which introduces a centrifugal potential that improves confinement. This boosts the viability of aneutronic fuels such as $p\,^{11}B$, where the required high energy regime for fusion presents a challenge to confinement. However, less is known about the distribution function of particles in a rotating mirror configuration compared to the standard non-rotating mirror. Characterizing this distribution could help in understanding effects in the confinement system such as instabilities.

We examine the steady state behavior of the particle distribution function, specifically near the loss cone boundary. Using finite-element simulations of the Fokker Planck diffusion equation on cold particle sources, we find an analytic approximation to the distribution function for a range of parameters. In particular, we investigate the distribution function's dependency on the confining potential and mirror ratio, as well as the regimes where typical distribution functions such as the Maxwellian with loss cone cutouts no longer sufficiently model the simulated results.

In this report, Section 2 introduces background on magnetic mirrors and the single-run simulation code developed by Dr. Ian Ochs. Section 3 explores models from previous literature, proposes a new model, and explicitly defines the methodology for comparison. Section 4 presents the results for error and best-fit parameters, and Section 5 discusses the implications and possible future work arising from this project.

2 Background

2.1 Magnetic Mirrors

Magnetic mirrors are magnetic confinement fusion devices that generally consist of a region of lower magnetic field strength bounded on both ends by regions of greater magnetic field strength. Particles gyrate on axial magnetic field lines, bouncing back and forth within the confines of the mirror if they fulfill certain velocity conditions at the plane of least magnetic field strength. However, particles that do not fulfill those conditions for velocity will escape. This inherent issue led to the magnetic mirror's decrease in popularity as the early successes of the tokamak drew increased attention.

We derive the mirror loss cone boundary here for later reference. We assume the adiabatic invariance of the magnetic moment μ.

$$\mu = \frac{w_\perp}{B} \tag{1}$$

where B is the magnetic field strength, $w_\perp = \frac{mv_\perp^2}{2}$, and $w_\parallel = \frac{mv_\parallel^2}{2}$. We assume conservation of energy and denote the arbitrary potential energy term as ϕ. Quantities without the additional subscripts are the quantities at the plane of least magnetic strength, while quantities with the subscript t are quantities at the particle's turning point.

$$\phi + w_\perp + w_\parallel = \phi_t + w_{\perp,t} + w_{\parallel,t} \tag{2}$$

Because we are assuming adiabatic invariance of the magnetic moment and the fact that t is the turning point, we can substitute $w_{\perp,t} = \frac{B_t}{B} w_\perp$ and $w_{\parallel,t} = 0$ in Eq. (2), and rearrange terms.

$$w_\parallel = (\phi_t - \phi) + \left(\frac{B_t}{B} - 1\right) w_\perp \tag{3}$$

To find the boundary condition, let $B_t = B_m$, the maximum magnetic field strength in the mirror. The quantity $\frac{B_m}{B}$ is the mirror ratio, R. Note that for the particle to be trapped, energy at B must be less than energy at B_m. Using this inequality, lumping all potential terms into ϕ, we can solve Eq. (3) in terms of $v_\perp$ and $v_\parallel$.

$$0 < \phi + (R-1)v_\perp^2 - v_\parallel^2 \tag{4}$$

$$\frac{v_\parallel^2 - \phi}{v_\perp^2} < R - 1 \tag{5}$$

Thus from Eq. (5), we observe that increasing the confining potential ϕ and the mirror ratio R lead to a greater range of velocities that are trapped. Particles with velocities that do not satisfy the inequality in Eq. (4) are said to be in the loss cone. Rotating the plasma introduces a centrifugal potential, which is desirable since it would increase confinement of particles in the mirror.

2.2 Single Run Simulation

The finite-element-based Fokker-Planck simulation code used to generate fit data was developed by Dr. Ian Ochs in Python. This section is a brief summary of the single run simulation set-up and code from Ochs et al. [1].

Given a mirror ratio R, confining potential ϕ, relativistic parameter χ, parallel diffusion coefficient $Z_{\parallel}$, and perpendicular diffusion coefficient $Z_{\perp}$, the single run simulation models the Fokker-Planck diffusion equation via a gmsh-generated mesh of momentum-space and finite elements solver DolfinX. The Dirichlet condition that particle flux is 0 at the loss cone boundary is imposed.

After specifying a source function for plasma particles dependent on source temperature T_s, the single run simulation numerically solves for the steady state distribution. It returns a normalized particle density distribution as a function of x (generalized dimensionless momentum) and θ (pitch angle).

We transform $x-\theta$ space to $x_{\parallel}-x_{\perp}$ space, where $x_{\parallel}$ and $x_{\perp}$ are the parallel and perpendicular dimensionless momentum components of x respectively using the following:

$$x_{\parallel} = x\cos(\theta) \qquad x_{\perp} = x\sin(\theta) \tag{6}$$

Thus, we reformulate the loss cone boundary condition in Eq. 4, with ϕ adjusting as necessary.

$$0 < \phi + (R-1)x_{\perp}^2 - x_{\parallel}^2 \tag{7}$$

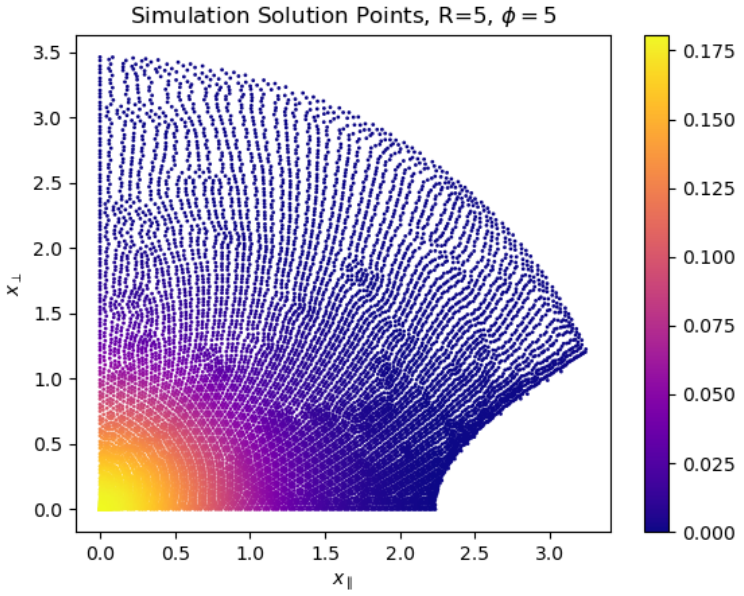

Fig. 1: single run simulation solution points for $R = 5, \phi = 5$

For this project, we choose the non-relativistic limit $\chi = 0.0$ and assume $Z_{\perp} = Z_{\parallel} = 1$. Our source function is the low temperature ($T_s = 0.01$) Maxwellian.

3 Methodology

3.1 Maxwell Model

One proposed model is the truncated Maxwellian, typically used for approximating the steady state distribution in standard non-rotating magnetic mirrors.

$$f_{max}(x_{\parallel}, x_{\perp}) = \mathbf{H}\left(\phi + (R-1)v_{\perp}^2 - v_{\parallel}^2\right) \cdot \pi^{-3/2} e^{-x_{\perp}^2 - x_{\parallel}^2} \tag{8}$$

where $\mathbf{H}$ is the Heaviside function and the other term is the normalized Maxwellian.

We note that as long as the loss cone boundary is far away from the bulk of the source particle distribution, the truncated Maxwellian is extremely close to being normalized. We expect this model to be a reasonable approximation of the steady state distribution function, considering the source function was also a Maxwellian.

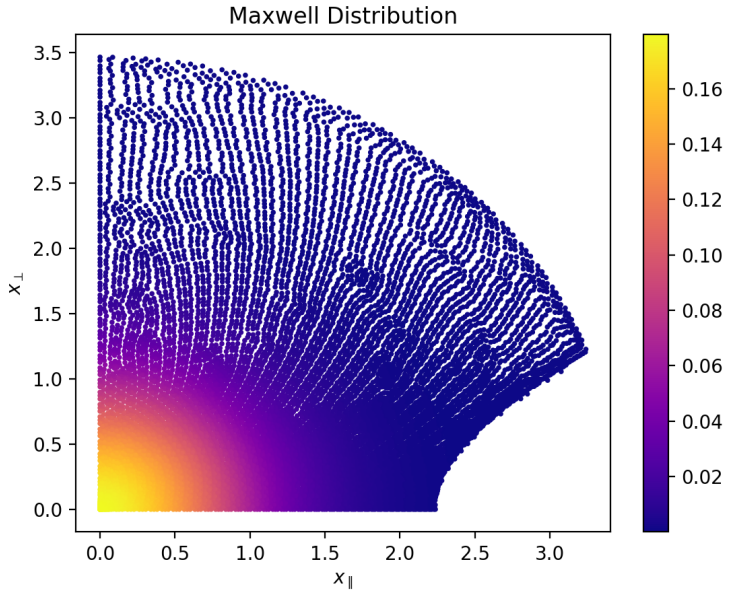

Fig. 2: Truncated Maxwellian in momentum space. Note, this is a close visual match to the single run simulation in Fig. 1.

3.2 Volosov Model

In 1973, Turikov studied steady state distribution functions, specifically with radial electric fields [2]. He cites a model by Volosov as follows:

$$f_v(v_{\parallel}, v_{\perp}) = \left[\frac{R-1}{R} v_E^2 + (R-1)v_{\perp}^2 - v_{\parallel}^2\right]^{1/2} e^{-\frac{v_{\perp}^2}{v^2}} \tag{9}$$

where v_E is the velocity of the frame of reference. We recast the Eq. 9 into the generalized momenta component coordinates and lump v_E into the confining potential term.

$$f_v(x_\parallel, x_\perp) = \Big[\underbrace{\phi + (R-1)x_\perp^2 - x_\parallel^2}_{\text{volosov loss cone prefactor}} \Big]^{1/2} e^{-\frac{x_\perp^2}{\bar{x}^2}} \tag{10}$$

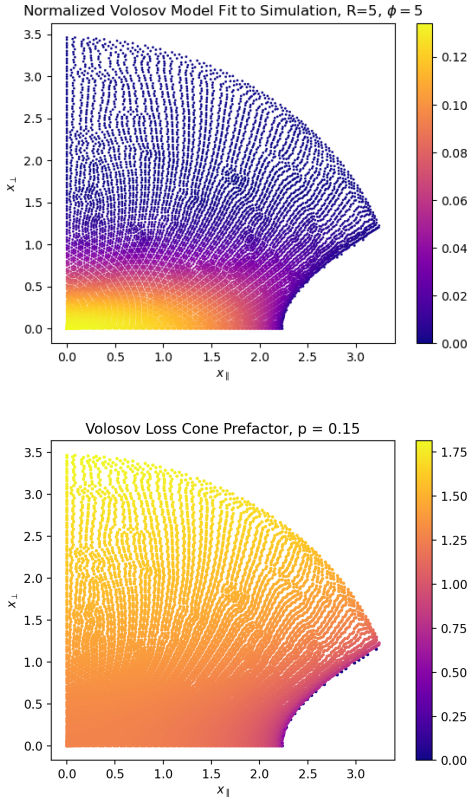

Fig. 3: (above) normalized volosov model is fitted to the simulation (below) the volosov prefactor is graphed for the power of 0.15

Fig. 3 (above) confirms Turikov's assessment: the Volosov model is not entirely realistic. The exponential term lacks a dependency on $x_\parallel$. However, we recognize the Volosov loss cone prefactor as the mirror loss cone boundary. When raised to a power between 0 and 1, the prefactor forces the model to smoothly approach 0 near the loss cone boundary as seen in Fig. 3 (below). This is an important behavior of the simulation with worse confinement (lower ϕ for example) that is not accounted for in a truncated Maxwellian. However, this prefactor does not describe behavior for low values of $x_\parallel$ and high values of $x_\perp$ accurately in that it grows instead of decays in those areas.

3.3 Proposed Model

We propose a model as follows, where x is as defined previously, with the relationship between x, $x_\perp$, and $x_\parallel$ explicitly written in Eq. 6.

$$f(x_\parallel, x_\perp) = \overbrace{\left(\mathbf{H}(\sqrt{\phi_0} - x) + e^{-\left(x-\sqrt{\phi_0}\right)/L}\mathbf{H}(x - \sqrt{\phi_0})\right)}^{\text{x decay prefactor}} \cdot \underbrace{\left(\phi + (R-1)x_\perp^2 - x_\parallel^2\right)^p}_{\text{volosov prefactor}} \underbrace{\mathbf{H}\left(\phi + (R-1)v_\perp^2 - v_\parallel^2\right) \cdot e^{-x_\perp^2 - x_\parallel^2}}_{\text{truncated Maxwellian}} \quad (11)$$

The truncated Maxwellian describes the bulk of the particles well for good confinement. We disregard the normalization factor of $\pi^{3/2}$ in the Maxwellian part because the model will be normalized before fitting. The Volosov prefactor is added to faciliate smooth transition to zero flux near the loss cone boundary. To correct for Volosov prefactor for problematic regions, we add this x decay prefactor that Dr. Ochs suggested. As seen in Fig. 4, past a certain $\sqrt{\phi_0}$ value, we introduce an exponential decay factor on the distribution function. A greater L value leads to a quicker decay.

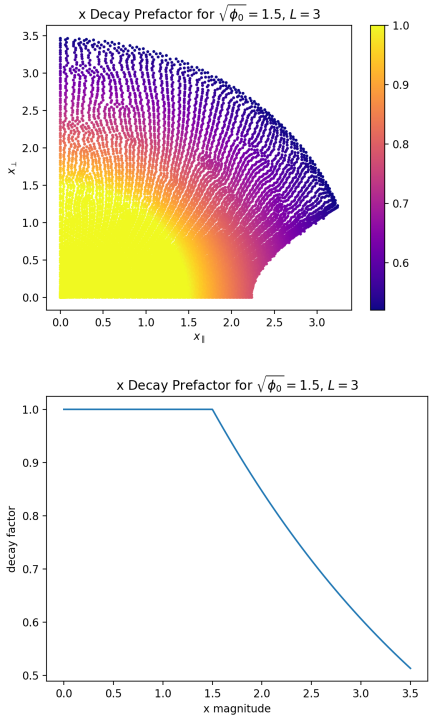

Fig. 4: (above) x decay prefactor in momentum space; (below) x decay prefactor as a function of x; both figures showcase the exponential decay past a certain x value

3.4 Comparison and Runs

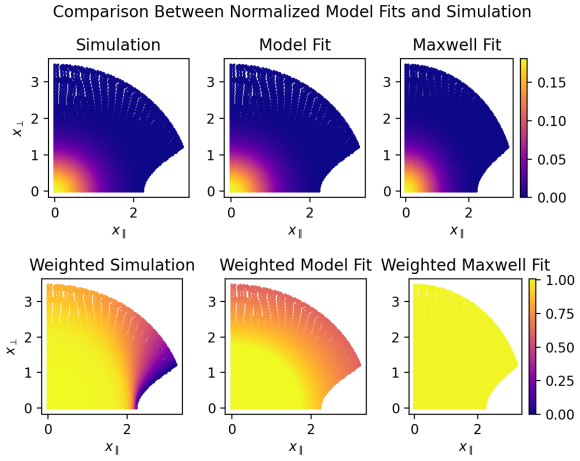

Fig. 5: (above) simulation and model fits for $R = 5, \phi = 5$; (below) weighted distributions by dividing solution points by f_{max}

The simulation and normalized model fits look the same, so we instead compare the distributions weighted against the Maxwell distribution. The weighted simulation looks like the Maxwell distribution except for the region close to the loss cone boundary, while the weighted truncated Maxwell model is unity everywhere. The weighted model fit has lower values for greater x magnitude like the weighted simulation does, indicating that it may be a better fit than the weighted Maxwell fit.

For each single run simulation, we remove points on the loss cone boundary since their values are 0. Because the models also have zero particle flux on the boundary, it is unnecessary to consider the boundary points during the fitting process. The simulation is already normalized.

To normalize, we evaluate the model at the mesh points, linear interpolating after taking into account the transformation from spherical coordinates (multiply distribution by $4\pi \cdot x_\perp^2$), and integrate in momentum space.

We use the following metric for error by summing over every mesh point:

$$E = \Sigma \left(f_{\text{simulation}} - f_{\text{model}}\right)^2 \tag{12}$$

We normalize the proposed model in Eq. 11, fit it to the simulation with the method of nonlinear least squares to find the best fit values for parameters $\sqrt{\phi_0}$, L, p, and calculate error. We also normalize the truncated Maxwell model and calculate error.

We repeat the procedure for two separate cases. The first case is fixed $R = 5$ and varying $\phi = \{3, 4, 5, 6, 7, 8\}$. The second case is fixed $\phi = 5$ and varying $R = \{5, 10, 15, 20\}$. We chose these values to cover typical cases in existing and proposed mirror plasmas.

4 Results

4.1 Fixed R, Varying ϕ

ϕ	**Model Fit Error**	**Maxwell Fit Error**	**Decreased Error**
3	7.6545e-03	1.2189e-01	93.72%
4	1.0963e-03	1.8743e-02	94.15%
5	1.4273e-04	2.8285e-03	94.95%
6	1.7192e-05	4.1197e-04	95.83%
7	2.0996e-06	6.0254e-05	96.52%
8	2.7173e-07	8.7764e-06	96.90%

Fig. 6: Error Calculations for Fixed R, Varying ϕ using the metric in Eq. 12

We run the case of $\phi = \{3, 4, 5, 6, 7, 8\}$ and fixed $R = 5$ for a total of 6 runs. Here, decreased error refers to the following calculation:

$$\frac{E_{\max} - E_{\text{model}}}{E_{\max}} \tag{13}$$

The accumulated model fit error across all 6 runs was 8.913e-03. The accumulated Maxwell fit error across all 6 runs was 1.439e-01. The accumulated decrease in error as a percentage is 93.81%, while the averaged decrease in error across the 6 runs is 95.13%.

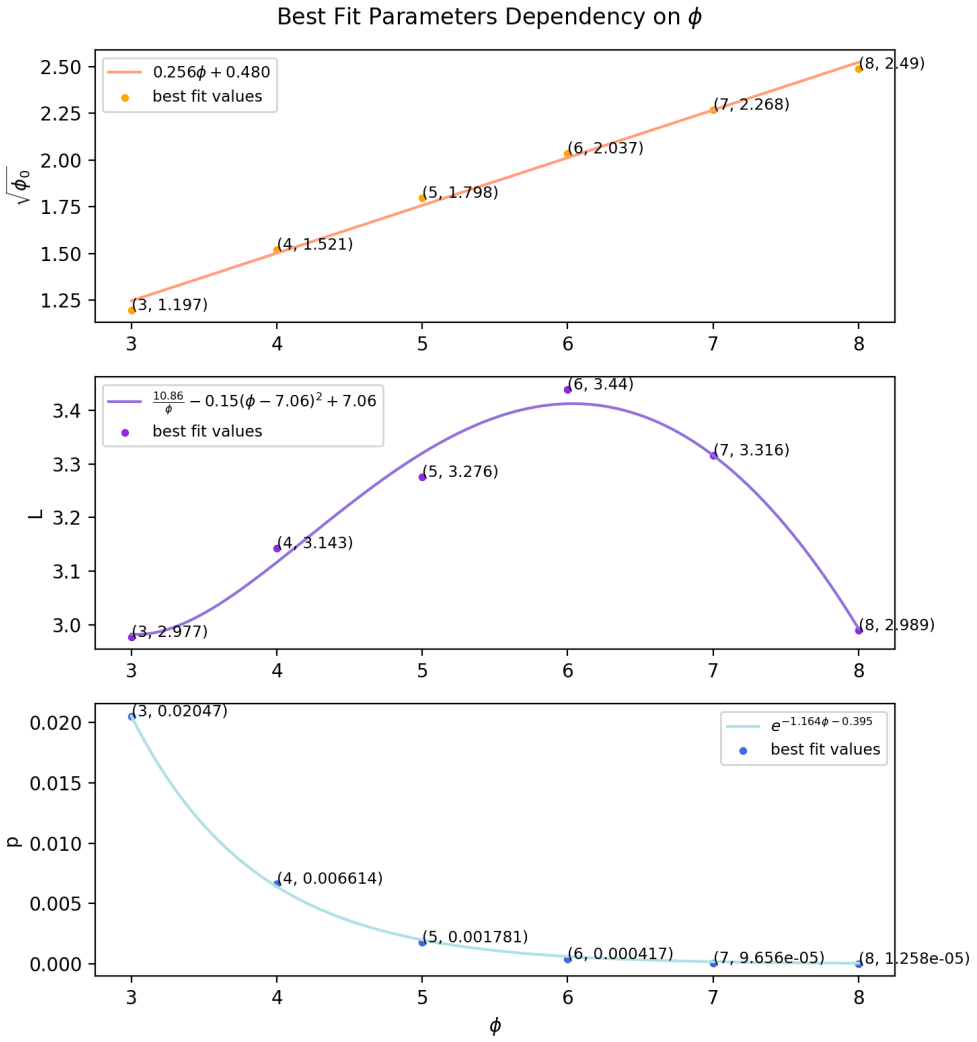

Fig. 7: Best Fit Parameters for Fixed R, Varying ϕ with Curve Fits

From Fig. 7, we see that the proportional dependencies of the best fit parameters on ϕ are as follows:

$$\sqrt{\phi_0} \approx 0.256\phi + 0.480 \Rightarrow \sqrt{\phi_0} \propto \phi \tag{14}$$

$$L \approx \frac{10.86}{\phi} - 0.15(\phi - 7.06)^2 + 7.06^* \Rightarrow L \propto \frac{1}{\phi} - \phi^2 + \phi \tag{15}$$

$$p \approx e^{-1.164\phi - 0.395} \Rightarrow p \propto e^{-\phi} \tag{16}$$

*L is admittedly not the best fit.

4.2 Fixed ϕ, Varying R

R	**Model Fit Error**	**Maxwell Fit Error**	**Decreased Error**
5	1.4273e-04	2.8285e-03	94.95%
10	1.1435e-04	1.7730e-03	93.55%
15	1.0157e-04	1.3945e-03	92.72%
20	1.0037e-04	1.2125e-03	91.72%

Fig. 8: Error Calculations for Fixed ϕ, Varying R using the metric in Eq. 12

We run the case of $R = \{5, 10, 15, 20\}$ and fixed $\phi = 5$ for a total of 4 runs. Decreased error in Fig. 8 refers to the same calculation in Eq. 13.

The accumulated model fit error across all 6 runs was 4.590e-04. The accumulated Maxwell fit error across all 6 runs was 7.209e-03. The accumulated decrease in error as a percentage is 93.63%, while the averaged decrease in error across the 4 runs is 93.32%.

From Fig. 9, we see that the proportional dependencies of the best fit parameters on R are as follows:

$$\sqrt{\phi_0} \approx 0.00496R + 1.774 \Rightarrow \sqrt{\phi_0} \propto R \tag{17}$$

$$L \approx \frac{1}{-0.530R + 1.586} + 4.214 \Rightarrow L \propto -\frac{1}{R} \tag{18}$$

$$p \approx \frac{1}{259.976R - 737.987} \Rightarrow p \propto \frac{1}{R} \tag{19}$$

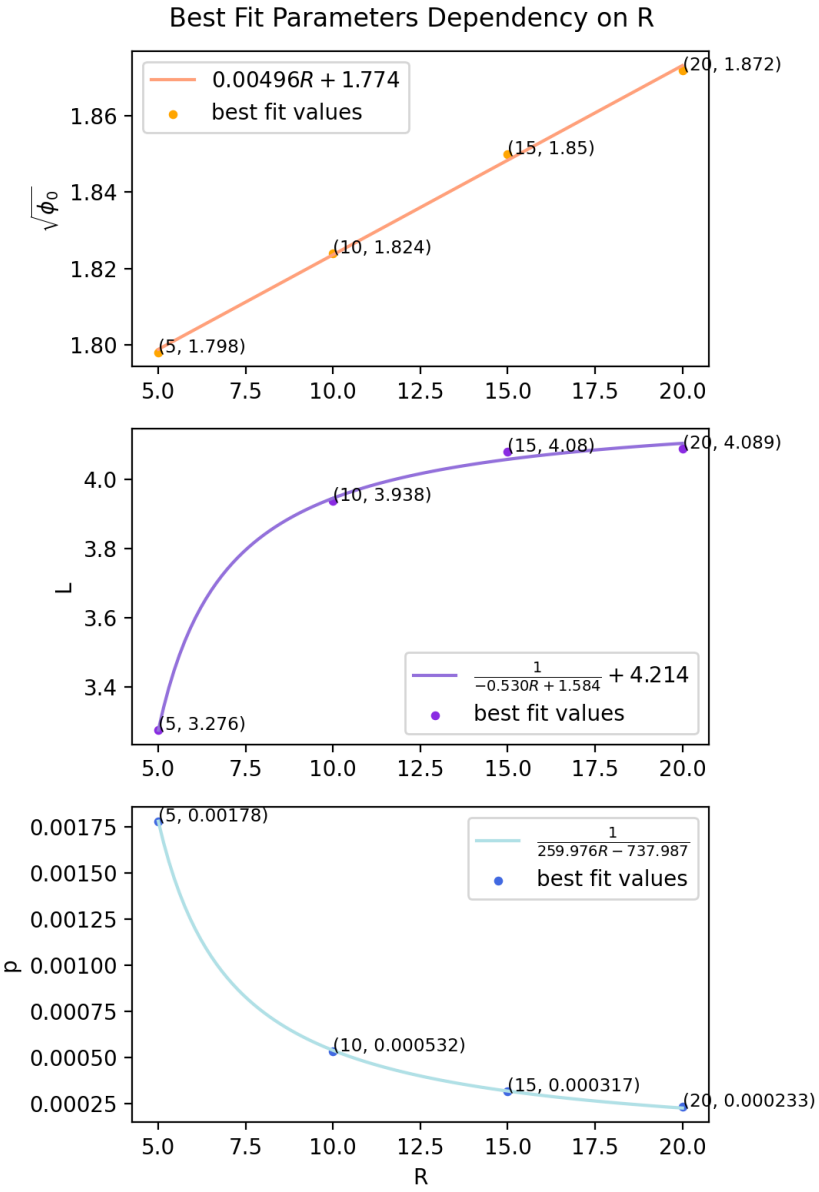

Fig. 9: Best Fit Parameters for Fixed ϕ, Varying R with Curve Fits

5 Discussion and Conclusion

We find that the proposed new model in Eq. 11 with the x Decay Prefactor, Volosov Loss Cone prefactor, and truncated Maxwellian factor performs better than the truncated Maxwellian model when fitted to the steady state distribution from the single run simulations. For better confinement with greater R or ϕ values, the parameter p, representing the best-fit power of the Volosov loss cone prefactor, has values of the magnitude 10^3 and less, while also decreasing exponentially (fixed $R = 5$) or inversely (fixed $\phi = 5$). This seems to indicate that the Volosov loss cone prefactor was not influential during the fitting process. Yet, the proposed model outperforms the truncated Maxwellian with an overall reduction of over 90% for both fixed $R = 5$ and $\phi = \{3, 4, 6, 7, 8\}$ and also fixed $\phi = 5$ and $R = \{5, 10, 15, 20\}$. If runs for other values of R and ϕ show the same trend of decreased error compared to the truncated Maxwellian, this model could be used as a rough baseline for comparison for newer models. Any future models should be able to outperform this model on the error metric in this report, thus also outperforming the standard truncated Maxwellian model in approximating the steady state distribution function for rotating plasmas in a magnetic mirror.

5.1 Future Work

The following improvements and future goals can be set:

- The Volosov Loss Cone prefactor does not seem to be a good fit in the range of $R \in [5, 20]$ and $\phi \in [3, 8]$ that we are interested in. Possibly the Volosov prefactor could be included for models for regions of significantly worse confinement, such as $\phi < 2$, or for fitting to the weighted distribution directly to capture the behavior near the loss cone boundary (Fig. 5 (below)).

- We would like to extend this procedure in the paper to evaluating models that generally approximate the steady state distribution function from the simulation and finding explicit dependencies of fit parameters on R and ϕ for $\chi = 0$.

- Possible further areas of interest would include the steady state distribution functions of relativistic plasmas, $\chi > 0$, which is important for understanding losses in high energy regimes for $p -^{11} B$ fusion.

6 Acknowledgements

Many thanks to postdoctoral fellows Dr. Elijah Kolmes and Dr. Ian Ochs for their generous guidance, Dr. Alexander Glasser for coding assistance, Professor Samuel Cohen for his administrative support with the internship program, and Professor Nathaniel Fisch for his mentorship support.

This work was made possible with support from the Program in Plasma Science and Technology, under US DOE contract number DE-AC02-09CH11466.

References

[1] I. E. Ochs, V. R. Munirov, and N. J. Fisch, "Confinement time and ambipolar potential in a relativistic mirror-confined plasma," Phys. Plasmas **30**, 052508 (2023).

[2] V. A. Turikov, "Effect of Electric Drift on the Loss Cone Plasma," in *Soviet Physics - Technical Physics*, vol. 18, no. 1, (1973).